NANO LETTERS

2005
Vol. 5, No. 5
905−911

Polymer Electrolyte Gating of Carbon Nanotube Network Transistors

Taner Ozel,[†,||] Anshu Gaur,[‡,||] John A. Rogers,[‡,§] and Moonsub Shim*[,‡]

Department of Physics, Department of Materials Science and Engineering, and Beckman Institute for Advanced Science and Technology, University of Illinois at Urbana-Champaign, Urbana, Illinois 61801

Received February 28, 2005; Revised Manuscript Received April 13, 2005

ABSTRACT

Network behavior in single-walled carbon nanotubes (SWNTs) is examined by polymer electrolyte gating. High gate efficiencies, low voltage operation, and the absence of hysteresis in polymer electrolyte gating lead to a convenient and effective method of analyzing transport in SWNT networks. Furthermore, the ability to control carrier type with chemical groups of the host polymer allows us to examine both electron and hole conduction. Comparison to back gate measurements is made on channel length scaling. Frequency measurements are also made giving an upper limit of ∼300 Hz switching speed for poly(ethylene oxide)/$LiClO_4$ gated SWNT thin film transistors.

Single-walled carbon nanotubes (SWNTs) have been studied intensively as prototypical 1D systems as well as potential high-performance materials to extend the capabilities of current microelectronics.[1] Their geometry-dependent electronic structure, ballistic transport and low power dissipation due to quasi one-dimensional transport, and their capability of carrying high current densities are some of the main reasons for the optimistic expectations for SWNTs.[1−6] Proof-of-concept devices such as field effect transistors (FETs),[7,8] logic circuits,[9,10] and sensors[11] have already been made. Recent advances in optical studies[12−14] are pushing the limits of SWNTs even further. However, device applications of individual SWNTs have been hindered by uncontrolled variations in characteristics. The device-to-device performance deviations arise from a distribution of diameter and chirality, variations at the metal contacts, and interactions with the substrate and the surrounding environment. One relatively new direction in SWNT electronics, which avoids some of these issues, is using networks of SWNTs where the ensemble average may provide uniformity from device to device.

To exploit the exceptional electronic properties of SWNTs in network-based devices, several challenges need to be overcome. The electronic inhomogeneity problem is currently being addressed by several research groups with selective chemistries for separating metallic tubes from semiconducting ones.[15,16] Other issues such as difficulties associated with n-channel operation in air,[17] role of contacts, highly environment sensitive performance, inefficient gating, and large hysteresis[18,19] remain largely unresolved. In single connection SWNT FETs, some of these issues have been addressed by using top gates with high-κ dielectric materials[20] or ultrathin gate oxides[9] and choice of contact metal.[21,22] Networks of SWNTs are appealing for applications such as large-area electronics especially because of their ease of fabrication, but many of these approaches require cumbersome and costly techniques. Recently, we have shown that polymer electrolytes can be used simultaneously to apply an electrostatic gate with nearly ideal efficiencies and to control charge carrier type in individual SWNT FETs.[23] Lu et al. have shown that polymer electrolyte gating can also be used with electron withdrawing molecular additives.[24] Polymer electrolyte gated FETs are very easy to fabricate and are therefore appealing for SWNT network TFTs. More importantly, polymer electrolyte gating eliminates hysteresis and short Debye lengths of the electrolyte solution can screen out many external effects (e.g., changes brought on by variations in gas adsorption from the ambient) providing a simple yet versatile method of studying electron transport in networks of prototypical 1D materials. Here, we first demonstrate that polymer electrolyte gating can be successfully applied to SWNT random networks then exploit it to examine how carrier transport in networks scales with device geometry. Measurements on complementary p- and n-devices and polymer electrolyte gating time response are also made to establish potential usefulness of SWNT network TFTs in macroelectronics.

Carbon nanotube TFTs were fabricated by catalytic chemical vapor deposition (CVD) on Si/SiO_2 substrates as described elsewhere.[19,25] Briefly, ferritin (Sigma, diluted 20 times in deionized water) was used to deliver catalysts for

* Corresponding author. E-mail: mshim@uiuc.edu.
† Department of Physics.
‡ Department of Materials Science and Engineering.
§ Beckman Institute for Advanced Science and Technology.
|| These authors contributed equally to this work.

10.1021/nl0503781 CCC: $30.25
Published on Web 04/26/2005

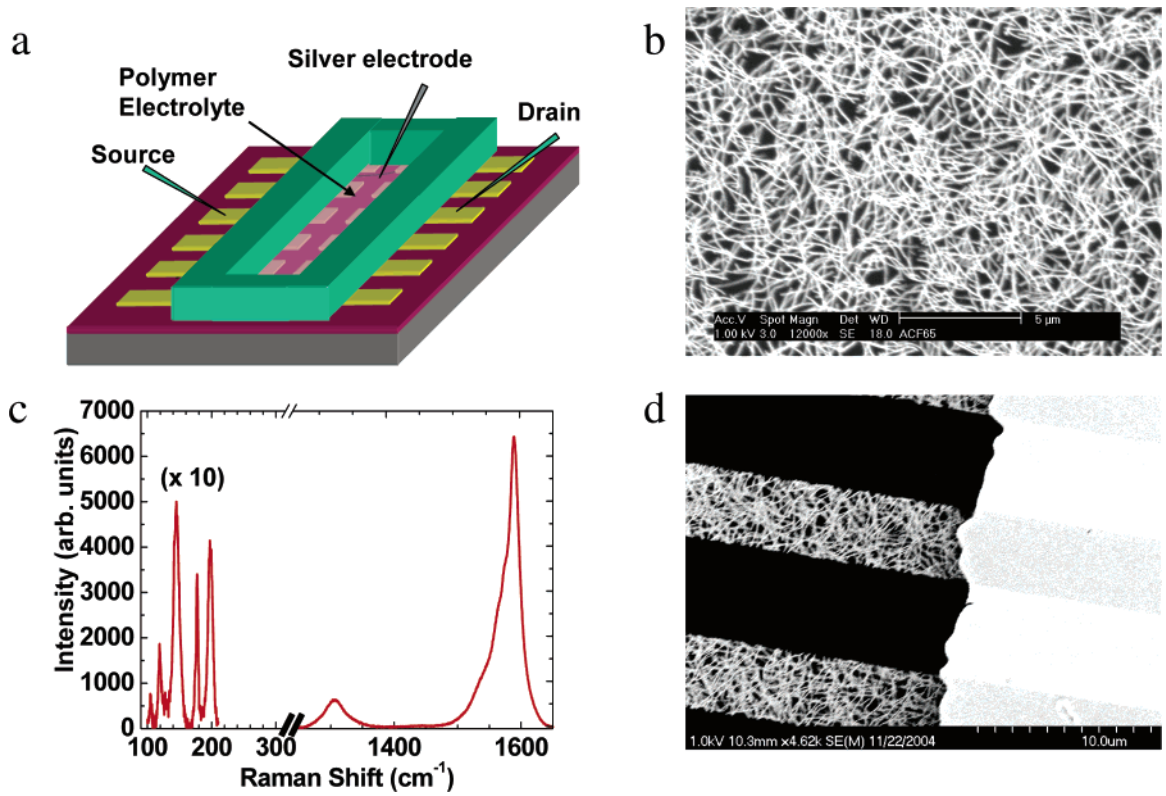

Figure 1. (a) Schematic of polymer electrolyte gate measurements on carbon nanotube networks. (b) SEM image showing a random network of carbon nanotubes. (c) Baseline corrected Raman spectrum of the SWNT film at 633 nm excitation. The radial breathing modes apparent correspond to diameters between 1 and 3 nm. (d) Low magnification SEM image showing a portion of the channel with striping geometry of a typical device.

nanotube synthesis at 900 °C with ultrahigh purity CH_4 and H_2. Nanotubes form a random network on the substrate which acts as an effective thin layer of semiconductor. Metal electrodes, Au (30 nm) with Cr (2 nm) adhesion layer, were deposited by electron beam evaporation. Following lift-off, equally spaced stripe patterns of SWNT networks along the channel length are obtained by second lithography step and O_2 plasma etch.[19] This stripe pattern prevents device-to-device cross-talk as well as the leakage to the silicon back gate. A Shipley 1805 photoresist was used for photolithography steps.[26] Two different types of polymer electrolytes were used as gate materials on top of SWNT TFTs, as discussed in the previous work for individual SWNT FETs.[23] Polymer electrolytes were made by directly dissolving $LiClO_4 \cdot 3H_2O$ in poly(ethylene oxide) (PEO, $M_n = 550$) or in polyethylenimine (PEI, $M_n = 800$) in air at room temperature with 2.4:1 and 1:1 polymer to salt weight ratios, respectively. The electrolytes were injected into a poly(dimethylsiloxane) fluidic channel over SWNT TFTs. The gate voltage was applied through a silver wire, which was dipped in the electrolyte as shown in Figure 1a. An SEM image of a typical SWNT network is shown in Figure 1b. Average nanotube density is about 6 μm^{-2}. The diameters of SWNTs vary between 1 and 3 nm as verified by Raman spectra[27] in Figure 1c and AFM imaging. The SEM image in Figure 1d shows patterned stripes of carbon nanotube network between drain and source electrodes.

The device characteristics of SWNT network TFTs operating with PEO- and PEI-based electrolytes are compared to back gate operation in Figure 2. Consistent with results of individual SWNTs, polymer electrolytes can be successfully employed on networks of SWNTs for highly efficient gating and controlling carrier type. Figure 2a shows transfer characteristics of a typical device with PEO electrolyte gating. The large hysteresis observed in the back-gate operation (inset) is eliminated. The same effect with n-channel rather than p-channel operation is observed with PEI-gating in Figure 2b. The inset is the transfer characteristics of the same device measured with back gate prior to polymer electrolyte addition. The efficiency of the polymer electrolyte gate is high enough that the transistors can operate at gate voltages that are an order of magnitude lower. Following Rosenblatt et al.,[28] we estimate the gate efficiency parameter to be ~0.6 from a subthreshold swing of ~100 mV/decade for 100 μm channel length devices. This gate efficiency parameter is smaller than that reported for PEO gating of individual SWNT[23] but may be due to small but nonzero residual off currents of ~0.25 nA in the network TFTs. The output characteristics for typical PEO and PEI electrolyte gated devices are shown in Figures 3a and 3b, respectively. Both p- (Figure 3c) and n-channel (Figure 3d) currents follow square law dependence on gate voltage. Following Durkop et al.[29] and assuming the total capacitance to be $C_T \approx 4 \times 10^{-3}$ F/m^2 (as discussed later), we estimate the corresponding saturation mobilities to be 21 cm^2/Vs for holes in PEO gating and 13.5 cm^2/Vs for electrons in PEI gating.

Because we are utilizing relatively high concentrations of electrolytes, possible leakage current from ionic conduction

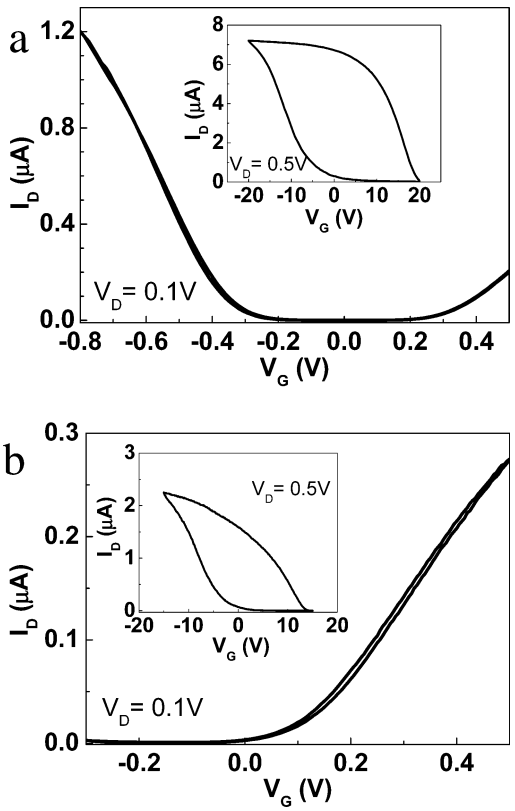

Figure 2. Transfer characteristics of PEO (a) and PEI (b) electrolyte gated SWNT TFTs. Insets are back gate transfer characteristics for corresponding devices before polymer electrolytes are placed. In the transfer curves the drain−source voltage is 0.1 V for the polymer−gate measurements, whereas it is 0.5 V for the back gate measurements. The device channel length is 100 μm and the width is 250 μm for both devices.

through the polymer electrolytes should be examined before further analysis of device characteristics. For comparison of p- and n-channel operation, whether doping via direct polymer-nanotube charge transfer or possible modification of the contacts by polymer adsorption on metal causes this change should also be carefully addressed. To test both ionic conduction and contact contributions, we have fabricated devices where the electrodes are covered with an insulating photoresist layer by an additional lithography step as shown in Figure 4a. Here, the direct contact between polymer electrolytes and the metal electrodes, which can change the metal work function and allow ionic conduction between drain and source electrodes (i.e., leakage current), is avoided. The inset in Figure 4b shows the back gate measurements of a SWNT network device with covered electrodes. No significant deviation in the device characteristics is observed after covering the electrodes. Operation of this device with polymer electrolytes is shown in Figure 4b. Similar on and off currents, transconductance, and p- to n-channel conduction conversion from PEO to PEI are observed with or without covered electrodes. These results are consistent with polymer chemical groups directly causing charge transfer to SWNTs (rather than effects at the contacts) and negligible contribution from ionic conduction in the measured current.

Polymer electrolyte gating with high efficiencies without the complications of hysteresis allows a more accurate analysis of device performance. To analyze device characteristics, we first estimate the gate capacitance (C_G) and the quantum (chemical) capacitance (C_Q) per unit area of the SWNTs as follows. Since C_G and C_Q are in series, the total capacitance is given by $C_T = (1/C_G + 1/C_Q)^{-1}$, and the smaller of C_G and C_Q dominates. C_G for polymer electrolytes may be given as $C_G = \epsilon\epsilon_o/\lambda$. The dielectric constant of the medium $\epsilon \sim 10$ (ref 30), and ϵ_o is the permittivity of free space. λ is the Debye length given by $\sqrt{\epsilon\epsilon_0 kT/2\rho e^2}$, where kT is the thermal energy and e is the electric charge. The concentrations (ρ) of the electrolytes used in our experiments are ~2.8 M and ~6.7 M for PEO/$LiClO_4$ and PEI/$LiClO_4$ electrolytes, respectively. Therefore, we estimate $C_G \sim 1$ F/m^2 for polymer electrolytes.

The quantum capacitance per unit area of the network can be estimated from the quantum capacitance per unit length (C_{Ql}) of individual SWNTs. For simplicity, we consider the network as parallel array of tubes. Per unit area quantity C_Q may then be thought of as the resultant capacitance of a number of parallel capacitors along the channel with capacitance C_{Ql} (i.e., the differential capacitance $C_Q\delta A$ in an area $\delta A = \delta w{\cdot}\delta l$ will be about the same as the resultant capacitance of δN parallel individual SWNTs along the length δl. Here, δw is the differential width. Thus, we have the following equality

$$C_Q\,\delta w{\cdot}\delta l \approx \delta N(C_{Ql}{\cdot}\delta l) = \left(\frac{\partial N}{\partial w}\delta w\right){\cdot}(C_{Ql}{\cdot}\delta l) \qquad (1)$$

which leads to the simple relation $C_Q \sim \partial N/\partial w\, C_{Ql}$. The linear density $\partial N/\partial w$ is estimated from the SEM images by randomly taking several linear cross sections and counting the total number of tubes that cross these sections. The linear density typically varies between 3 μm^{-1} and 10 μm^{-1}. Mobilities are calculated using the value, $\partial N/\partial w \sim 10\,\mu$m^{-1}, which should give conservative estimates. Due to the assumptions mentioned above, the mobility values are rough estimates but the length scaling trend is the same regardless of the actual value of $\partial N/\partial w$ since the same constant value is used to calculate the mobilities for all polymer gating measurements. With $C_{Ql} \sim 4e^2/\pi\hbar v_F \approx 4 \times 10^{-10}$ F/m when only one subband is occupied,[28] quantum capacitance per unit area is $\sim 4 \times 10^{-3}$ F/m^2. Since $C_Q \ll C_G$, the total capacitance $C_T \approx C_Q \approx 4 \times 10^{-3}$ F/m^2 for polymer electrolyte gating. For back gate, $C_G \approx \epsilon\epsilon_o/t \approx 3.5 \times 10^{-4}$ F/m^2 (where t is the thickness of the oxide layer and $\epsilon \sim 3.9$) is an order of magnitude smaller than C_Q and leads to $C_T \approx C_G$.

Assuming diffuse transport, the carrier mobility can then be estimated from the relation

$$\mu \approx \left|\frac{\partial I_D}{\partial V_G}\right| \frac{L}{wC_TV_D} \qquad (2)$$

where L is the channel length and w is the channel width. The entire physical width of the channel is used to calculate device mobilities with eq 2 for all data presented here. Using an effective width of the sum of SWNT stripes will lead to

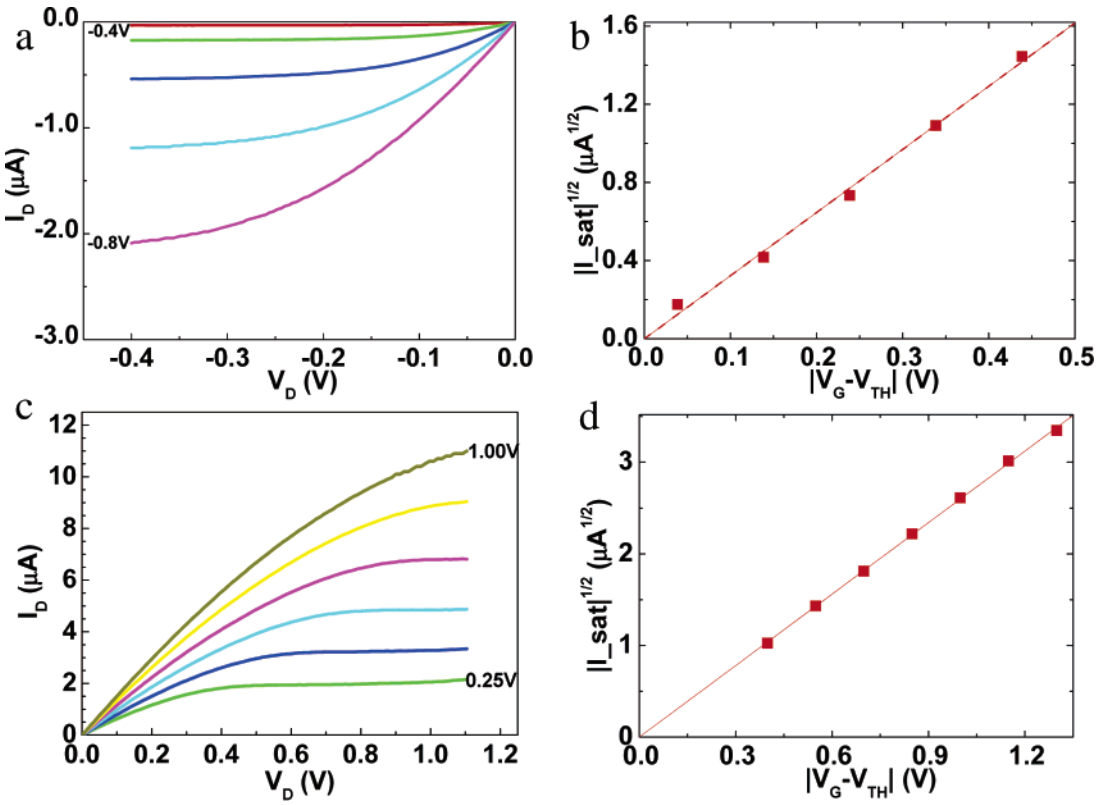

Figure 3. Output characteristics of PEO (a) and PEI (b) electrolyte gated SWNT TFTs. The square dependence of saturation current on gate voltage can be seen for both PEO and PEI gated devices in (c) and (d), respectively. The device geometries are the same as the devices shown in Figure 2.

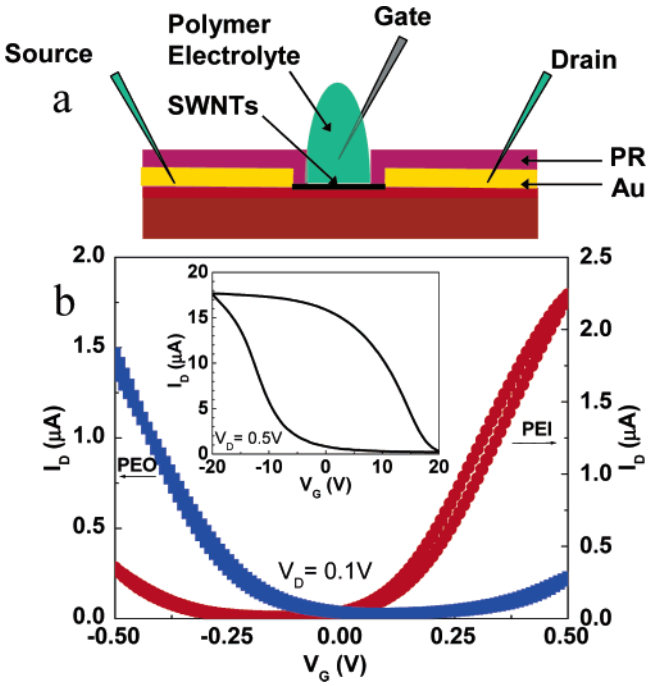

Figure 4. Schematic of polymer electrolyte gate measurement with covered electrodes (a) and transfer characteristics with PEO and PEI electrolytes (b). Inset in (b) is the back gate transfer characteristics with covered electrodes before polymer electrolyte addition. The channel lengths and widths are the same as the devices shown in Figure 2.

mobilities that are about twice as high, representing values that may be achieved with optimized stripe geometries. For our PEO electrolyte gated devices, hole mobility varies from 10 to 40 cm^2/Vs. These mobilities estimated from our PEO electrolyte gate measurements are in agreement with back-gate measurements for long channel lengths ($L > 10$ μm). The effective per tube mobility[31] calculated from the device mobility range of ~10 to 40 cm^2/Vs measured for PEO gating corresponds to ~1300 to 5300 cm^2/Vs, which is within the typical hole mobility range of 1000 to 6000 cm^2/Vs reported for back gated single tube transistors.[17,21,28] Similar analysis on PEI electrolyte gating measurements leads to same length scaling behavior with electron mobilities that are slightly smaller (by about a factor of 2) than the hole mobilities measured with PEO electrolyte gate for the entire channel length scale studied here.

With the effectiveness of polymer electrolyte gating on networks of SWNTs established and with estimates of relevant capacitances, we now address performance scaling with device geometry. Figure 5a compares the transconductance in the linear regime vs L for back, PEO, and PEI gating. In the long channel limit ($L > 10$ μm), the same qualitative behavior is observed for all three cases. The offset for back gating is due to the difference in gate capacitance (i.e., the inefficient back gating leads to transconductance that is about an order of magnitude smaller). The lower left inset, which compares the linear hole mobility, shows nearly identical scaling in the long channel limit. The ratio of on-current to off-current (on/off ratio) shown in Figure 5b also indicates that all three gating results exhibit similar saturation behavior past $L \sim 30$ μm. The decay of on/off ratio at short lengths

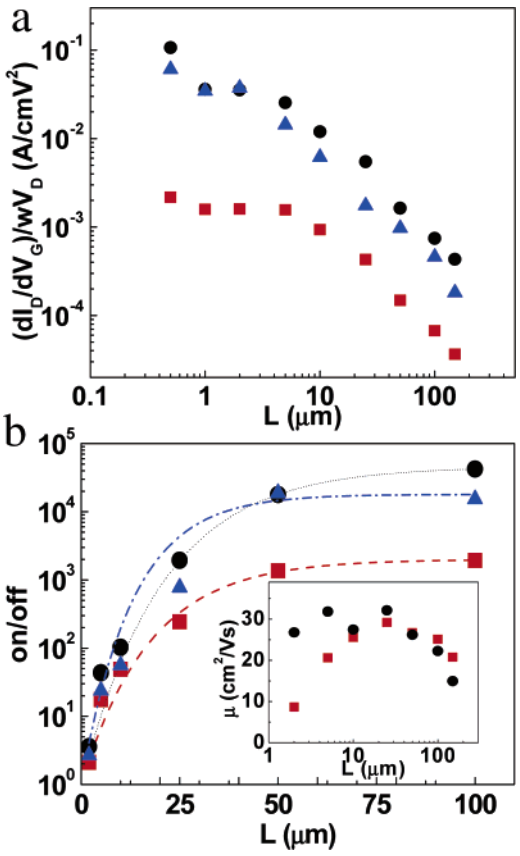

Figure 5. (a) Scaling of drain−source voltage and channel width normalized transconductance in the linear regime with channel length for back gate (square), PEO (circle), and PEI (triangle) electrolyte gates. Note that all channel widths are 250 μm except for two shortest channel lengths (0.5 and 1 μm), which have widths of 10 μm. (b) On/off current ratio scaling with channel length for back gate (square), PEO (circle), and PEI (triangle) electrolyte gates for a different set of devices with same device geometry. Dashed lines are guides to eye. The inset shows the hole mobility scaling with channel length calculated from transconductance and capacitances discussed in the text. The mobility values are obtained by averaging two sets of devices to improve accuracy. Note that these are the device mobilities calculated using the entire channel width rather than effective widths of the nanotube network stripes.

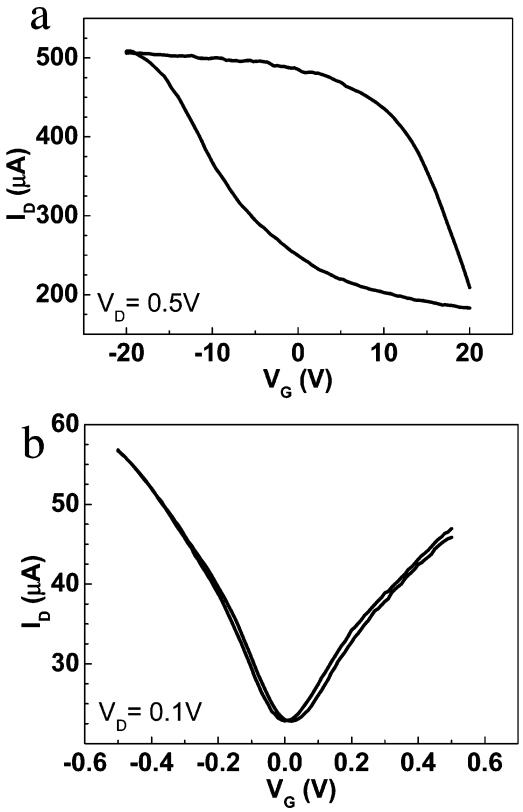

Figure 6. Comparison of transfer characteristics measured by back (a) and PEO electrolyte (b) gating on the same 2 μm channel length device.

is due to percolation of all metallic tube pathways. Note that pathways composed only of small band gap semiconductors or a mixture of metals and small gap semiconductors may also contribute to increasing off current, but for simplicity we may refer to these paths also as all metallic pathways at room temperature. Due to higher percentage of semiconducting tubes (~70%), the probability of all metal pathways quickly diminishes at long channel lengths. Since each path has tubes in series, the tube with the highest resistance (i.e., semiconductors when they are turned off) will dominate, leading to an effective semiconductor behavior. We note that 2 orders of magnitude higher resistance of metal-semiconductor junctions compared to metal−metal or semiconductor-semiconductor junctions[32] should significantly reduce the contributions from pathways that consist of a mixture of metallic and semiconducting tubes to the on-current.

As the channel length decreases, distinctly different behavior is seen at $L \sim 10$ μm, which is comparable to the average tube length. Due to the transition from transport via interconnected tube network to conduction through tubes that directly span the channel, fundamentally different behavior is expected when length scale approaches the average tube length. However, there is an additional deviation in the measured transconductance between back gating and polymer electrolyte gating. This discrepancy in the short channel limit can also be seen in the device mobility in the inset of Figure 5b where PEO electrolyte gating leads to nearly constant mobility with channel length, whereas large decrease is seen in back gating. Measurements at each channel length shown in Figure 5 are made on the same devices, and therefore this discrepancy between the two gating methods is not likely to be arising from network to direct connection transition.

When the channel length is comparable or smaller than the average tube length, transport through tubes that directly span source to drain leads to small channel resistance and the contact resistance may become important. In these devices, the electrodes are made of Au with Cr adhesion layer and we can consider Cr to be the contact metal. In this case, the Fermi level pinning should lead to Schottky contacts.[33] The observed length dependence in back gating may then result from Schottky barrier limited transport (there may also be contributions from tunnel barriers at the contacts). In polymer electrolyte gating, the Schottky barrier should in principle become transparent because of the short depletion layer widths due to highly efficient band bending afforded by short Debye lengths of the electrolyte solution. Qualitatively same length scaling of electron (PEI gating) and hole (PEO gating) transport and ambipolar behavior observed for PEO gating (Figures 2a and 6b) but not for back gating (Figures 2a inset

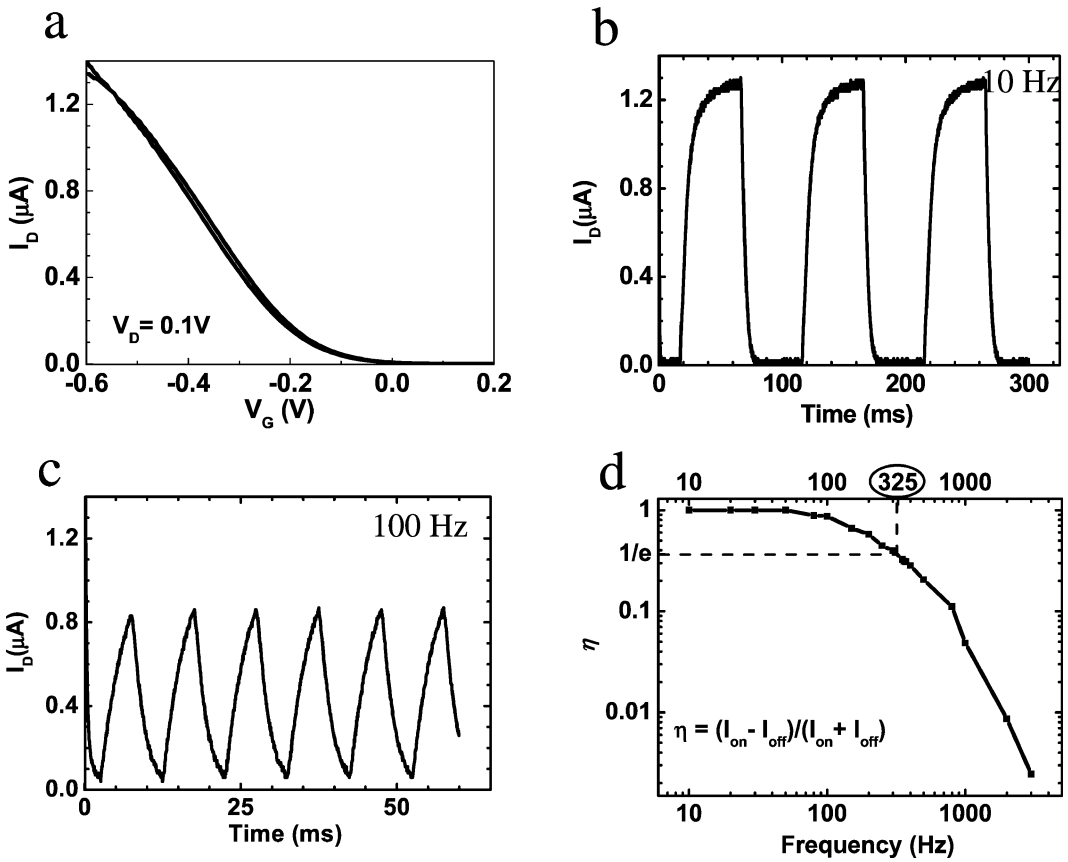

Figure 7. Frequency measurements on PEO electrolyte gated SWNT TFT. (a) Transfer characteristics. Panels (b) and (c) are the drain current response to square wave pulse gate voltage for 10 Hz and 100 Hz, respectively. (d) The parameter η (defined in the text) at different frequencies for the device with transfer characteristics shown in (a). A square wave pulse (−0.6 V, 0 V) is applied to PEO electrolyte gate.

and 6a) further support this idea. These observations are consistent with contact resistance contributing significantly to the apparent carrier mobility decrease in back gate measurements at short channel lengths.

However, direct comparison of the transfer characteristics of short channel devices suggests that other effects may give rise to the discrepancy between back and polymer electrolyte gating. Figure 6 compares the transfer characteristics of the same 2 μm channel SWNT TFT operating under back (a) and PEO electrolyte (b) gate. The transconductance at positive gate voltages for forward sweep (negative to positive) decreases significantly and the current never quite reaches a minimum in back gating, whereas a distinct minimum and the onset of n-channel conduction is seen for PEO-gating. Contribution from contact resistance should appear largely as limited on-current and is unlikely to account for this observation. Comparison of back and polymer gating in Figure 6 suggests that there may be a significant reduction in back gate efficiency at short channel lengths. It is most likely that a combination of differences in contact resistances as well as in gate efficiencies gives rise to the observed divergent behavior between back and electrolyte gating of short channel devices. While further studies are required to elucidate these deviations arising at short channel lengths, polymer electrolyte gating of SWNT TFTs seems to conform better to expectations based on characteristics of individual tubes (i.e., nearly constant mobility at short channel lengths).

Several advantages in polymer electrolyte gating of SWNT networks have been shown here: (1) high gate efficiencies, (2) lack of hysteresis, (3) the ability to achieve both p- and n-channel conduction, and (4) simple method of studying length scaling of device performance. However, one obvious drawback of polymer electrolyte gating is the switching speed limited by ionic mobility of the gate medium rather than the carrier mobility of the semiconductor material. To estimate the upper limit of the switching speed, we have examined the time response of SWNT network TFTs. Figure 7 shows the response of a 100 μm channel PEO-gated TFT. The responses are measured by applying square-wave gate pulses with amplitude separation of 0 and −0.6 V at varying frequencies. As shown in the transfer characteristics in Figure 7a, the device is on at −0.6 V and off at 0 V. Figures 7b and 7c show the response of the drain current as the TFT is switched on and off at frequencies of 10 and 100 Hz, respectively. The difference in the magnitude of the separation between on and off currents decreases as the switching frequency increases. To quantify switching speed, we introduce the parameter $\eta = I_{on}-I_{off}/I_{on}+I_{off}$. η is 1 when the device can be completely turned off and 0 when the device cannot be turned off at all. This parameter η is plotted as a function of gate voltage frequency in Figure 7d. The cutoff (1/e) frequency of the device shown in Figure 7 is 325 Hz, which is surprisingly fast. This switching speed should be close to the upper limit for the PEO/$LiClO_4$ system

since we are using low molecular weight polymer which is liquid at room temperature (i.e., conditions similar to that for the highest achievable ionic mobility for this electrolyte system). We note that the definition of the cutoff frequency may be different depending on the application needs. However, the device can be completely switched off even at 50 Hz.

We have shown that highly efficient polymer electrolyte gating can be successfully applied to SWNT networks. Qualitatively different behavior between back and polymer electrolyte gating at short channel lengths has been shown, suggesting that polymer electrolyte gating may be a valuable and a very simple method of characterizing nanoscale semiconductor devices. The ability to control the mode of operation from p- to n-type demonstrates the versatility of polymer electrolytes beyond efficient gate media. Switching speed of ∼300 Hz has also been measured for PEO electrolyte gated SWNT network TFTs, giving an estimate of the upper limit for these devices. Polymer electrolyte gated SWNT TFTs may be a cost-effective solution for many developing electronics without demanding speed requirements such as electronic paper displays.

Acknowledgment. This work was supported by DARPA-funded AFRL-managed Macroelectronics Program Contract FA8650-04-C-7101, the NSF (grant no. NIRT-0403489 and DMR-0348585), and ACS PRF. Atomic force microscopy and scanning electron microscopy of the samples were carried out at the Center for Microanalysis of Materials, University of Illinois, which is partially supported by the U.S. Department of Energy under grant DEFG02-91-ER45439.

References

(1) Avouris, Ph.; Appenzeller, J.; Martel, R.; Wind, S. J. *Proc. IEEE* **2003**, *91*, 1772.
(2) Saito, R.; Dresselhaus, G.; Dresselhaus, M. S. *Physical Properties of Carbon Nanotubes*; Imperial College Press: London, 1998.
(3) Dresselhaus, M. S.; Dresselhaus, G.; Saito R. *Phys. Rev. B* **1992**, *45*, 6234.
(4) Mintmire, J. W.; Dunlap, B. I.; White C. T. *Phys. Rev. Lett.* **1992**, *68*, 631.
(5) Dekker, C. *Phys. Today* **1999**, *52*, 22.
(6) McEuen, P. L.; Fuhrer, M. S.; Park, H. K. *IEEE Trans. Nanotechnol.* **2002**, *1*, 78.
(7) Tans, S. J.; Verschueren, A. R. M.; Dekker, C. *Nature* **1998**, *393*, 49.
(8) Martel, R.; Schmidt, T.; Shea, H. R.; Hertel, T.; Avouris Ph. *Appl. Phys. Lett.* **1998**, *73*, 2447.
(9) Derycke, V.; Martel, R.; Appenzeller, J.; Avouris, Ph. *Nano Lett.* **2001**, *1*, 453.
(10) Bachtold, A.; Hadley, P.; Nakanishi, T.; Dekker, C. *Science* **2001**, *294*, 1317.
(11) Kong, J.; Franklin, N. R.; Zhou, C.; Chapline, M. G.; Peng, S.; Cho, K.; Dai, H. *Science* **2000**, *287*, 622.
(12) Htoon, H.; O'Connell, M. J.; Cox, P. J.; Doorn, S. K.; Klimov, V. I. *Phys. Rev. Lett.* **2004**, *93*, 027401.
(13) Hartschuh, A.; Pedrosa, H. N.; Novotny, L.; Krauss, T. D. *Science* **2003**, *301*, 1354.
(14) Arnold, M. S.; Sharping, J. E.; Stupp, S. I.; Kumar, P.; Hersam, M. C. *Nano Lett.* **2003**, *3*, 1549.
(15) Balasubramanian, K.; Sordan, R.; Burghard, M.; Kern, K. *Nano Lett.* **2004**, *4*, 827.
(16) An, L.; Fu, Q.; Lu, C.; Liu, J. *J. Am. Chem. Soc.* **2004**, *126*, 10520.
(17) Shim, M.; Javey, A.; Kam, N. W. S.; Dai, H. *J. Am. Chem. Soc.* **2001**, *123*, 11512.
(18) Snow, E. S.; Novak, J. P.; Campbell, P. M.; Park, D. *Appl. Phys. Lett.* **2003**, *82*, 2145.
(19) Zhou, Y. X.; Gaur, A.; Hur, S. H.; Kocabas, C.; Meitl, M. A.; Shim, M.; Rogers, J. A. *Nano Lett.* **2004**, *4*, 2031.
(20) Javey, A.; Kim, H.; Brink, M.; Wang, Q.; Ural, A.; Guo, J.; McIntyre, P.; McEuen, P. L.; Lundstrom, M.; Dai, H. *Nature Materials* **2002**, *1*, 241.
(21) Javey, A.; Guo, J.; Wang, Q.; Lundstrom, M.; Dai, H. *Nature* **2003**, *424*, 654.
(22) Yaish, Y.; Park, J. Y.; Rosenblatt, S.; Sazonova, V.; Brink, M.; McEuen, P. L. *Phys. Rev. Lett.* **2003**, *92*, 046401.
(23) Siddons, G. P.; Merchin, D.; Back, J. H.; Jeong, J. K.; Shim, M. *Nano Lett.* **2004**, *4*, 927.
(24) Lu, C. G.; Fu, Q.; Huang, S. M.; Liu, J. *Nano Lett.* **2004**, *4*, 623.
(25) Shim, M.; Siddons, G. P. *Appl. Phys. Lett.* **2003**, *83*, 3564.
(26) Metal electrodes for 0.5 μm and 1 μm long channels were patterned with 6% poly(methyl methacrylate) in anisole using deep UV light source. The rest of the lithography steps were same as long channel devices using Shipley 1805 resist.
(27) Bachilo, S. M.; Strano, M. S.; Kittrell, C.; Hauge, R. H.; Smalley, R. E.; Weisman, R. B. *Science* **2002**, *298*, 2361.
(28) Rosenblatt, S.; Yaish, Y.; Park, J.; Gore, J.; Sazanova, V.; McEuen, P. L. *Nano Lett.* **2002**, *2*, 869.
(29) Durkop, T.; Getty, S. A.; Cobas, E.; Fuhrer, M. S. *Nano Lett.* **2004**, *4*, 35−39.
(30) Gray, F. M. *Solid Polymer Electrolytes*; VCH Publishers: New York, 1991.
(31) For a simple estimate of the per tube mobility, we factor in the effective width (i.e., the sum of the widths of the SWNT stripes) and consider that only ∼1.5% of the each of the stripe width consists of tubes. This fill factor of 1.5% comes from the estimate that there are only about 10 tubes per 1 μm and that the average diameter of the tubes is ∼1.5 nm. These two factors give per tube mobility as $\mu_{\text{tube}} = 2\mu_{\text{device}}/0.015$.
(32) Fuhrer, M. S.; Nygard, J.; Shih, L.; Forero, M.; Yoon, Y. G.; Mazzoni, M. S. C.; Choi, H. J.; Ihm, J.; Louie, S. G.; Zettl, A.; McEuen, P. L. *Science* **2000**, *288*, 494.
(33) Leonard, F.; Tersoff, J. *Phys. Rev. Lett.* **1999**, *83*, 5174.

NL0503781